Adaptive Generalized Super-Twisting Tracking Control of an Underwater Vehicle

Bent O. A. Haugaløkken[1], Herman B. Amundsen[1,2,†], Håkon S. Fadum[2], Jan T. Gravdahl[2], Sveinung J. Ohrem[1]

***Abstract*— Tracking control for unmanned underwater vehicles is essential, both for autonomous operations and complex tasks where the vehicle is manually controlled by a pilot. Underwater vehicles are typically subjected to perturbations due to environmental effects such as ocean currents and waves. Moreover, obtaining an accurate model of the vehicle dynamics is highly challenging. This introduces a need for a model-free control system that is robust to such perturbations. In this paper, we propose the use of two higher-order sliding mode controllers, the generalized super-twisting algorithm (GSTA) and the adaptive GSTA, for 4 degree-of-freedom control of an underwater vehicle. The stability of the closed loop system is analyzed through Lyapunov theory and the performance of the controllers is evaluated in a set of full-scale field trials at an aquaculture facility. The results show that the controllers outperform classical PID control.**

Fig. 1: SINTEF ACE Rataren, a full-scale laboratory facility designed for development and testing of aquaculture technologies. Photo: M. O. Pedersen, SINTEF Ocean.

I. Introduction

Unmanned underwater vehicles (UUVs) such as remotely operated vehicles (ROVs) and autonomous underwater vehicles (AUVs) are important for monitoring and interacting in underwater environments where humans cannot or should not travel [1]. The oceans present a challenging and unforgiving environment where the vehicle is subjected to harsh disturbances from currents and waves. Due to various hydrodynamic effects, it can be challenging to model underwater vehicles accurately. This is particularly the case for ROVs, as the many cavities and appendages on the body make it difficult to calculate the damping and added mass effects of the vehicle. Perturbations due to environmental loads and model uncertainties thus introduce the need for robust control techniques for UUVs. Aquaculture is one industry that has a need for robust control of underwater vehicles. In aquaculture, ROVs are typically used for inspection, maintenance, and repair operations in fish farms [2], where the vehicle must operate in the wave-zone, in complex and irregular current flows [3] and in close proximity to flexible net cages [4].

Sliding mode control (SMC) is a robust method for controlling perturbed dynamic systems that are affected by matched uncertainties and perturbations [5]. SMC achieves its robustness to these types of perturbations through a signum function which introduces a discontinuity to the control law. However, due to phenomena such as time delays and hysteresis, this discontinuity in the control law can introduce high-frequency oscillations known as chattering to physical systems. Chattering can be avoided by replacing the signum function with a saturation or sigmoid function [5]. However, this restricts the sliding system's trajectories from reaching the sliding surface but instead its vicinity and thus reduces robustness to disturbances [6]. Another way to deal with the chattering effects is to apply higher-order sliding mode (HOSM) techniques, which ensure convergence of the system's sliding variable and its derivatives to zero even when affected by disturbances and uncertainties [6], [7].

One powerful HOSM technique is the super-twisting algorithm (STA) [8], which avoids chattering and generates smooth control inputs by placing the discontinuous term behind an integrator. The main disadvantage of STA is that it requires known bounds of the disturbances. To overcome this disadvantage, STA controllers that adapt their gains have been suggested [6], [9], with the main benefit that they can be robust to perturbations with unknown bounds. Moreover, an alternative HOSM technique called the generalized STA was developed in an attempt to deal with uncertain control coefficients and perturbations that are both state- and time-dependent [10], [11]. Underwater vehicles are affected by such uncertainties through, e.g., the inertia moment due to added mass effects [12], and through control coefficients due to vortex effects stemming from the thrusters. In [13], an adaptive GSTA control law is proposed that combines the state- and time-dependent robustness property of GSTA with adaptive STA's robustness to perturbations of unknown bounds. The GSTA control law has successfully been applied

[1]Dept. of Aquaculture, SINTEF Ocean, Trondheim, 7010, Norway
[2]Dept. of Engineering Cybernetics, Norwegian University of Science and Technology, Trondheim, 7034, Norway
[†]Corresponding author: herman.b.amundsen@ntnu.no

for underwater vehicles such as AUV [14] and underwater snake robots [13], [15], in addition to other types of vehicles (e.g., spacecraft [16] and quad-copters [17]). In [14], GSTA was successfully applied in sea trials for an AUV to control depth and yaw.

In this paper, GSTA and adaptive GSTA is proposed for 4 degree-of-freedom (DOF) control of an ROV, based on the work of [18]. The main contribution of the paper is an experimental validation of two variations of GSTA through field trials. The field trials were conducted at an industrial-scale fish farm (see Fig. 1). The controllers were implemented on an ROV that performed an autonomous inspection of fish cage nets where the vehicle was commanded to autonomously move along the net at a desired depth while maintaining a desired distance, heading, and velocity relative to the net [19]. The performance of the GSTA controllers is compared to each other and to a classic PID controller, demonstrating good performance. Finally, the paper also proves analytically that the tracking errors converge to the origin in finite time.

The paper is outlined as follows. Section II contains the vehicle model. Section III presents the GSTA control technique and the adaptive law used for estimating the adaptive gains, in addition to a stability analysis of the control system. The navigation and guidance systems for the vehicle can be found in Section IV. The experimental setup for the field trials is presented in Section V and Section VI contains the results from the trials. The results are discussed and the control performances are compared in Section VII. Finally, Section VIII holds the conclusions for this work.

II. Vehicle Model

The ROV considered in this paper is described in 4 DOFs (surge, sway, heave and yaw). A kinematic model represented in the North-East-Down (NED) reference frame $\{n\}$ is employed, while the dynamics are described in the body-fixed reference frame $\{b\}$. The following assumptions are introduced:

Assumption 1. *The vehicle is port-starboard, fore-aft, and bottom-top symmetric.*

Remark 1. *Diagonality in the inertia and damping matrices follows from Assumption 1 [12].*

Assumption 2. *The vehicle is passively stabilized in roll and pitch. Thus, these DOFs can be neglected and considered to be null.*

Assumption 3. *The center of gravity (CG) and center of buoyancy (CB) are located along the same vertical axis in* $\{b\}$.

Assumption 4. *The center of origin (CO) of the body-fixed reference frame is placed in CG.*

Remark 2. *Assumptions 3-4 imply that the buoyancy and gravitational forces are only present in the heave-direction, and simplify the centripetal and Coriolis matrix [12].*

The 4 DOF vehicle model is expressed by the following control plant model [12]

$$\dot{\boldsymbol{\eta}} = \boldsymbol{J}(\boldsymbol{\eta})\boldsymbol{\nu} \tag{1}$$

$$\boldsymbol{M}\dot{\boldsymbol{\nu}} + \boldsymbol{C}(\boldsymbol{\nu})\boldsymbol{\nu} + \boldsymbol{D}(\boldsymbol{\nu})\boldsymbol{\nu} + \boldsymbol{g} = \boldsymbol{\tau} + \boldsymbol{w}, \tag{2}$$

where $\boldsymbol{\eta} = [x, y, z, \psi]^T$ is the generalized position vector, and $\boldsymbol{\nu} = [u, v, w, r]^T$ contains the linear and angular velocities of the vehicle. The term $\boldsymbol{\nu}$ is decomposed in $\{b\}$ and thus $\boldsymbol{J}(\eta) = [\boldsymbol{R}_z(\psi), 0; \boldsymbol{0}_{1x3}, 1]$ is the transformation matrix from $\{b\}$ to $\{n\}$, where $\boldsymbol{R}_z(\psi) \in \mathbb{R}^{3x3}$ is the principal rotation matrix around the z-axis. Furthermore, $\boldsymbol{M} = \boldsymbol{M}_{RB} + \boldsymbol{M}_A > 0, \in \mathbb{R}^{4\times4}$ is the system inertia matrix, which is the sum of the rigid-body mass matrix and the added mass matrix, $\boldsymbol{C}(\boldsymbol{\nu}) = \boldsymbol{C}_{RB}(\boldsymbol{\nu}) + \boldsymbol{C}_A(\boldsymbol{\nu}) \in \mathbb{R}^{4\times4}$ contains the rigid body and added mass centripetal and Coriolis forces, and $\boldsymbol{D}(\boldsymbol{\nu}) = \boldsymbol{D}_l + \boldsymbol{D}_n(\boldsymbol{\nu}) > 0, \in \mathbb{R}^{4\times4}$ is the damping matrix made up of a linear and nonlinear part. Due to Assumption 1, $\boldsymbol{M}$ and $\boldsymbol{D}(\boldsymbol{\nu})$ are diagonal, while $\boldsymbol{C}(\boldsymbol{\nu})$ can be calculated from $\boldsymbol{M}$ according to [12] as

$$\boldsymbol{C}(\boldsymbol{\nu}) = \begin{bmatrix} 0 & 0 & 0 & -m_{22}v \\ 0 & 0 & 0 & m_{11}u \\ 0 & 0 & 0 & 0 \\ m_{22}v & -m_{11}u & 0 & 0 \end{bmatrix}, \tag{3}$$

where m_{ii} refers to element ii of $\boldsymbol{M}$. The gravitational and buoyancy forces are represented by the vector $\boldsymbol{g} = [0, 0, g_z, 0]^T$, while the control forces are contained in $\boldsymbol{\tau} \in \mathbb{R}^4$. Finally, the perturbations from wave-excitation forces, the unknown current flow, and unmodeled dynamics are lumped together in the disturbance vector $\boldsymbol{w} \in \mathbb{R}^4$. We also make the following assumptions on the control forces and disturbance vector:

Assumption 5. *The vehicle is fully actuated.*

Assumption 6. *The disturbance vector* $\boldsymbol{w}$ *is upper and lower bounded.*

III. Control Design and Stability Analysis

A. Control objective

The control objective is to track reference signals in heading, depth, and surge and sway velocity. This can be formulated as

$$\lim_{t\to\infty} \boldsymbol{x}_1(t) = \lim_{t\to\infty} \begin{bmatrix} \tilde{u}(t) \\ \tilde{v}(t) \\ \tilde{z}(t) \\ \tilde{\psi}(t) \end{bmatrix} = \boldsymbol{0}, \tag{4}$$

where $\tilde{u} \triangleq u - u_d$, $\tilde{v} \triangleq v - v_d$, $\tilde{z} \triangleq z - z_d$, $\tilde{\psi} \triangleq \psi - \psi_d$ are the tracking errors, and $\boldsymbol{x}_1 \in \mathbb{R}^4$ is a vector of tracking errors. Here, ψ_d, z_d, u_d, v_d are the time-varying reference signals in heading, depth, and surge and sway velocity.

Assumption 7. *The reference signals* u_d, v_d, z_d, ψ_d *and their derivatives wrt. time are Lipschitz continuous.*

B. The sliding variable

To utilize sliding mode, we first need to define a sliding surface $\boldsymbol{\sigma}$, which is to be designed such that if $\boldsymbol{\sigma} = \mathbf{0}$, then the error dynamics are asymptotic stable, and such that the control input $\boldsymbol{\tau}$ appear in the first derivative of $\boldsymbol{\sigma}$. Consider the following choice for the sliding variable

$$\boldsymbol{\sigma} = \boldsymbol{x}_1 + \begin{bmatrix} \dot{\tilde{u}} \\ \dot{\tilde{v}} \\ 2\tilde{w} + \dot{\tilde{w}} \\ \tilde{r} \end{bmatrix} = \boldsymbol{x}_1 + \boldsymbol{x}_2. \tag{5}$$

For $\boldsymbol{\sigma} = \mathbf{0}$, this yields

$$\begin{bmatrix} \dot{\tilde{u}} \\ \dot{\tilde{v}} \\ \dot{\tilde{w}} \\ \dot{\tilde{r}} \end{bmatrix} = \begin{bmatrix} \dot{\tilde{u}} \\ \dot{\tilde{v}} \\ \ddot{\tilde{z}} \\ \dot{\tilde{\psi}} \end{bmatrix} = \begin{bmatrix} -\tilde{u} \\ -\tilde{v} \\ -2\dot{\tilde{z}} - \tilde{z} \\ -\tilde{\psi} \end{bmatrix}, \tag{6}$$

which is linear and Hurwitz, thus making $\boldsymbol{x}_1 = \mathbf{0}$ an exponentially stable equilibrium point.

We now want to rearrange (5) on the form

$$\dot{\boldsymbol{\sigma}} = \boldsymbol{\varphi}_1(\boldsymbol{\sigma}, t) + \boldsymbol{\varphi}_2(\boldsymbol{\sigma}, t) + \boldsymbol{\Gamma}(\boldsymbol{\sigma}, t)\boldsymbol{\tau}, \tag{7}$$

where $\boldsymbol{\varphi}_1(\boldsymbol{\sigma}, t)$ are the vanishing terms bounded by $||\boldsymbol{\varphi}_1(\boldsymbol{\sigma}, t)|| < \rho||\boldsymbol{\varphi}_1(\boldsymbol{\sigma})||$ for some $\rho > 0$, $\boldsymbol{\varphi}_2(\boldsymbol{\sigma}, t)$ is a vector of non-vanishing state and time-dependent perturbation terms, and $\boldsymbol{\Gamma}(\boldsymbol{\sigma}, t)$ is a matrix of the control coefficients.

Defining a reference vector

$$\boldsymbol{\nu}_r = \begin{bmatrix} u_r \\ v_r \\ w_r \\ r_r \end{bmatrix} = \begin{bmatrix} u_d - \dot{\tilde{u}} \\ v_d - \dot{\tilde{v}} \\ w_d - \tilde{w} - \tilde{z} - \dot{\tilde{w}} \\ r_d - \tilde{\psi} \end{bmatrix}, \tag{8}$$

and inserting it into (5), gives

$$\begin{aligned} \boldsymbol{\sigma} &= \begin{bmatrix} u - (u_d - \tilde{u}) \\ v - (v_d - \tilde{v}) \\ w - (w_d - \tilde{w} - \tilde{z} - \dot{\tilde{w}}) \\ r - (r_d - \tilde{\psi}) \end{bmatrix} = \begin{bmatrix} u - u_r \\ v - v_r \\ w - w_r \\ r - r_r \end{bmatrix} \\ &= \boldsymbol{\nu} - \boldsymbol{\nu}_r \ . \end{aligned} \tag{9}$$

Furthermore, differentiation of (9) gives

$$\begin{aligned} \dot{\boldsymbol{\sigma}} = \dot{\boldsymbol{\nu}} - \dot{\boldsymbol{\nu}}_r = \\ \boldsymbol{M}^{-1}\left(-\boldsymbol{D}(\boldsymbol{\nu})\boldsymbol{\nu} - \boldsymbol{C}(\boldsymbol{\nu})\boldsymbol{\nu} - \boldsymbol{g} + \boldsymbol{\tau} + \boldsymbol{w}\right) - \dot{\boldsymbol{\nu}}_r \ , \end{aligned} \tag{10}$$

where it is clear that $\boldsymbol{\tau}$ is present. We can now write (10) on the form of (7) where

$$\begin{aligned} \boldsymbol{\varphi}_1(\boldsymbol{\sigma}, t) &= -\boldsymbol{M}^{-1}\left(\boldsymbol{D}(\boldsymbol{\nu})\boldsymbol{\nu} + \boldsymbol{C}(\boldsymbol{\nu})\boldsymbol{\nu}\right) \\ &= -\boldsymbol{M}^{-1}\left(\boldsymbol{D}(\boldsymbol{\sigma} + \boldsymbol{\nu}_r) + \boldsymbol{C}(\boldsymbol{\sigma} + \boldsymbol{\nu}_r)\right)(\boldsymbol{\sigma} + \boldsymbol{\nu}_r) \end{aligned} \tag{11}$$

are the vanishing perturbation terms,

$$\boldsymbol{\varphi}_2(\boldsymbol{\sigma}, t) = \boldsymbol{M}^{-1}(-\boldsymbol{g} + \boldsymbol{w}) - \dot{\boldsymbol{\nu}}_r \tag{12}$$

are the non-vanishing perturbation terms, and

$$\boldsymbol{\Gamma}(\boldsymbol{\sigma}, t) = \boldsymbol{\Gamma} = \boldsymbol{M}^{-1} \tag{13}$$

is the control coefficients matrix. We note that the system in (10) has matched uncertainties due to the matrix $\boldsymbol{\Gamma}$.

C. Control law

1) The generalized super-twisting algorithm: Based on [10], we propose the following fixed-gain GSTA controller:

$$\boldsymbol{\tau} = -\boldsymbol{K}_1\boldsymbol{\phi}_1(\boldsymbol{\sigma}) + \boldsymbol{z} \tag{14}$$

$$\dot{\boldsymbol{z}} = -\boldsymbol{K}_2\boldsymbol{\phi}_2(\boldsymbol{\sigma}) \ , \tag{15}$$

where

$$\boldsymbol{\phi}_1(\boldsymbol{\sigma}) = \lceil\boldsymbol{\sigma}\rfloor^{\frac{1}{2}} + \boldsymbol{\beta}\sigma \tag{16}$$

$$\boldsymbol{\phi}_2(\boldsymbol{\sigma}) = \frac{1}{2}\lceil\boldsymbol{\sigma}\rfloor^0 + \frac{3}{2}\boldsymbol{\beta}\lceil\boldsymbol{\sigma}\rfloor^{\frac{1}{2}} + \boldsymbol{\beta}^T\boldsymbol{\beta}\boldsymbol{\sigma} \tag{17}$$

and $\boldsymbol{K}_1 = \boldsymbol{K}_1^T > 0$, $\boldsymbol{K}_2 = \boldsymbol{K}_2^T > 0$ and $\boldsymbol{\beta} = \boldsymbol{\beta}^T > 0$ are constant, positive definite design matrices in $\mathbb{R}^{4x4}$. Furthermore, $\lceil\boldsymbol{\sigma}\rfloor^a \in \mathbb{R}^4$ is the vector whose i-th element is defined as

$$\lceil\sigma_i\rfloor^a = |\sigma_i|^a \text{sgn}(\sigma_i). \tag{18}$$

2) The adaptive generalized super-twisting algorithm: An alternative to the fixed-gain GSTA (14)-(15) is to allow for the gain matrices $\boldsymbol{K}_1, \boldsymbol{K}_2$ to be updated through the use of an adaptive law. In accordance with the proposed adaptive laws in [13], $\boldsymbol{K}_1, \boldsymbol{K}_2$ are diagonal matrices whose i-th elements are updated according to

$$\dot{k}_{1,i} = \begin{cases} 0, & \text{if } |\sigma_i| < \alpha_{\text{tol}} \\ \omega_1\sqrt{\frac{\gamma_1}{2}}, & \text{otherwise,} \end{cases} \tag{19}$$

$$\dot{k}_{2,i} = 2\epsilon k_{1,i} + \lambda + 4\epsilon^2 \ . \tag{20}$$

Here, $\omega_1, \gamma_1, \varepsilon, \lambda \in \mathbb{R}$ are positive constants. Furthermore, $\alpha_{\text{tol}} \in \mathbb{R}$ in (19) is a small positive constant operating as a tolerance for when σ_i is considered to be large enough for changes to occur in the estimation of $k_{1,i}$. Without this modification, $k_{1,i}$ will experience a constant change because $\sigma_i = 0$ is unlikely to occur in real systems. The key idea is here to allow the system to stay on the sliding manifold by updating the gains instead of relying on well-tuned fixed gains without a need for an estimate of the bounds of the perturbations and control coefficients.

D. Stability analysis

Before analyzing the stability of the proposed control law (14)-(15) with and without the adaptation (19)-(20), we make the following assumptions about the system (10) [13].

Assumption 8 (Continuity condition)**.** *The function $\boldsymbol{\varphi}(\boldsymbol{\sigma}, t) = \boldsymbol{\varphi}_1(\boldsymbol{\sigma}, t) + \boldsymbol{\varphi}_2(\boldsymbol{\sigma}, t)$ is Lipschitz continuous with respect to t, and $\boldsymbol{\varphi}(\boldsymbol{\sigma}, t) \in \mathcal{C}^1$ with respect to $\boldsymbol{\sigma}$.*

Assumption 9 (Bounded disturbance)**.** *The uncertain control coefficient matrix is assumed to be bounded by positive constraints:*

$$0 < k_m \leq \lambda_{min}\left(\boldsymbol{\Gamma}\right) \leq \lambda_{max}\left(\boldsymbol{\Gamma}\right) \leq k_M. \tag{21}$$

Assumption 10 (Vanishing perturbation)**.** *The perturbation term $\boldsymbol{\varphi}(\boldsymbol{\sigma}, t)$ can be split into two parts as follows: $\boldsymbol{\varphi}(\boldsymbol{\sigma}, t) = \boldsymbol{\varphi}_1(\boldsymbol{\sigma}, t) + \boldsymbol{\varphi}_2(\boldsymbol{\sigma}, t)$, such that the first term is*

vanishing at the origin, i.e., $\boldsymbol{\varphi}_1(\mathbf{0},t) = \mathbf{0} \forall t \geq 0$*, and is bounded by*

$$||\boldsymbol{\varphi}_1(\boldsymbol{\sigma},t)|| \leq \rho||\boldsymbol{\varphi}_1(\boldsymbol{\sigma})||,\ \rho > 0. \tag{22}$$

Assumption 11 (Bounded growth for $\boldsymbol{\varphi}_2$ wrt. to $\boldsymbol{\sigma}$)**.** *The total time derivative of the non-vanishing component of the perturbation term divided by the control coefficient matrix* $\boldsymbol{\Gamma}$ *can be represented as:*

$$\begin{gathered}\frac{d}{dt}\left(\boldsymbol{\Gamma}^{-1}\boldsymbol{\varphi}_2(\boldsymbol{\sigma},t)\right) = \\ \boldsymbol{\Gamma}^{-1}\frac{\partial \boldsymbol{\varphi}_2}{\partial t} - \boldsymbol{\Gamma}^{-2}\boldsymbol{\varphi}_2\frac{\partial \boldsymbol{\Gamma}}{\partial t} + \left(\boldsymbol{\Gamma}^{-1}\frac{\partial \boldsymbol{\varphi}_2}{\partial \boldsymbol{\sigma}} - \boldsymbol{\Gamma}^{-2}\boldsymbol{\varphi}_2\frac{\partial \boldsymbol{\Gamma}}{\partial \boldsymbol{\sigma}}\right)\dot{\boldsymbol{\sigma}} = \\ \boldsymbol{\delta}_1(\boldsymbol{\sigma},t) + \boldsymbol{\delta}_2(\boldsymbol{\sigma},t)\dot{\boldsymbol{\sigma}}\end{gathered} \tag{23}$$

where $\boldsymbol{\delta}_1(\boldsymbol{\sigma},t)$ *and* $\boldsymbol{\delta}_2(\boldsymbol{\sigma},t)$ *are bounded by positive constants:*

$$||\boldsymbol{\delta}_1(\boldsymbol{\sigma},t)|| \leq \bar{\delta}_1,\ ||\boldsymbol{\delta}_2(\boldsymbol{\sigma},t)|| \leq \bar{\delta}_2. \tag{24}$$

We now introduce Theorem 1, which states the stability properties of the GSTA controller with fixed gains.

Theorem 1. *Suppose that* $\boldsymbol{\Gamma}$ *and* $\boldsymbol{\varphi}(\boldsymbol{\sigma},t)$ *in* (10) *satisfy Assumptions 8-11. Then, the states* $\boldsymbol{x}_1$ *and* $\boldsymbol{x}_2$ *converge to zero and* $\boldsymbol{z}$ *converges to* $-\boldsymbol{\varphi}(\boldsymbol{\sigma},t)$*, globally and in finite-time, if GSTA gains* $\boldsymbol{K}_1, \boldsymbol{K}_2$ *and* $\boldsymbol{\beta} > 0$ *are designed in accordance with [11].*

Proof. The proof is given in [11]. □

Inspired by [6] and [13], the stability properties of the GSTA control law with adaptive gains are given by Theorem 2.

Theorem 2. *Suppose that* $\boldsymbol{\Gamma}$ *and* $\boldsymbol{\varphi}(\boldsymbol{\sigma},t)$ *in* (10) *satisfy Assumptions 8-11. Then, the states* $\boldsymbol{x}_1$ *and* $\boldsymbol{x}_2$ *converge to zero and* $\boldsymbol{z}$ *converges to* $-\boldsymbol{\varphi}(\boldsymbol{\sigma},t)$*, globally and in finite-time, if gains* $\boldsymbol{K}_1$ *and* $\boldsymbol{K}_2$ *are designed as expressed in* (19)-(20)*, with* $\beta > 0, \lambda > 0, \omega_1 > 0, \gamma_1$ *and* $\epsilon = \frac{\omega_2}{2\omega_1}\sqrt{\frac{\gamma_2}{\gamma_1}}$*, where* $\omega_2 > 0$ *and* $\gamma_2 > 0$*.*

Proof. The proof is given in [13]. □

IV. Navigation and Guidance System

To test the proposed control laws, they were implemented as part of an autonomous system for inspecting aquaculture net pens. The navigation and guidance system is based on [19] and is briefly summarized here.

The objective of the net-following system is to move along the net with a given distance $d_d(t) > 0$ and speed $U_d(t) > 0$, and a heading normal to the net structure. A front-facing Doppler velocity log (DVL) sensor is mounted to the fore of the vehicle. Based on the measured length of the four hydroacoustic DVL beams, the net in front of the DVL is approximated as a plane, from which one can calculate the minimal distance d between the plane and the CO, and the normal vector ψ_{net} to the net.

A line-of-sight (LOS) guidance law [12], [19] is used to calculate desired course angle for the ROV according to

$$\chi_{\text{LOS}} = \gamma_p - \arctan\left(\frac{y_e}{\Delta}\right)\ , \tag{25}$$

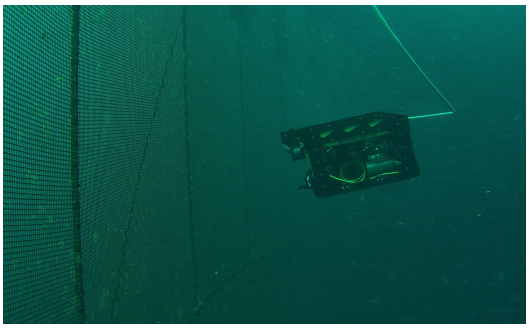

Fig. 2: Argus Mini ROV performing net-following with DVL.

where $\gamma_p \triangleq \psi_{\text{net}} + \frac{\pi}{2}$ is the angle tangential to the plane (or $\gamma_p \triangleq \psi_{\text{net}} - \frac{\pi}{2}$ if commanded towards port), $y_e \triangleq d - d_d$ is the distance error, and $\Delta > 0, \in \mathbb{R}$ is the lookahead distance [12]. Moreover, the desired velocities in surge and sway are given as [19]

$$u_d = U_d \cos(-\psi + \chi_{LOS}) \tag{26}$$

$$v_d = U_d \sin(-\psi + \chi_{LOS})\ . \tag{27}$$

Finally, the desired heading is equal to the net normal angle, i.e., $\psi_d \triangleq \psi_{\text{net}}$, and the desired depth $z_d(t)$ is set by the operator.

V. Experimental Setup

Field trials were conducted in May 2022 at SINTEF ACE Rataren, a full-scale laboratory facility for testing aquaculture technologies outside Trondheim, Norway (see Fig. 1). In the field trials, an Argus Mini ROV equipped with a Nortek 1000 DVL was used. The ROV performing net-following is depicted in Fig. 2.

The ROV was placed inside a fish cage and was set to traverse the net at a distance of $d_d = 3$ m. The fish cage was stocked with about 200 000 salmon, which is known to decrease the performance of DVLs due to scattering of acoustic signals [20]. The desired depth was chosen to setpoints between 3.5 m to 5 m, while the desired speed was set to $U_d = 0.2$ m/s. Three case studies were performed in total, GSTA with fixed and adaptive gains and a PID controller.

The ROV was equipped with a DVL for measurement of velocities, a depth sensor for measurement of depth, a fluxgate compass for measurement of heading, and a gyro for measurement of angular velocity. An extended Kalman filter (EKF) based on [21] was used for estimating the vehicle states, while appropriate reference models were utilized for generating smooth reference signals [12].

S

VI. Results

A. Case study 1: GSTA

The first case study presents the performance of the GSTA controller during a net-following field trial. The gains used for the GSTA controller are found in Tab. I while Fig. 3 shows the resulting plot containing the vehicle's net distance, total speed (i.e., norm of surge and sway velocity), surge

TABLE I: GSTA Controller gains

Degree of freedom	k_1	k_2	β
Surge	0.5	5	5
Sway	1	1	10
Depth	25	0.001	15
Heading	2	0.008	25

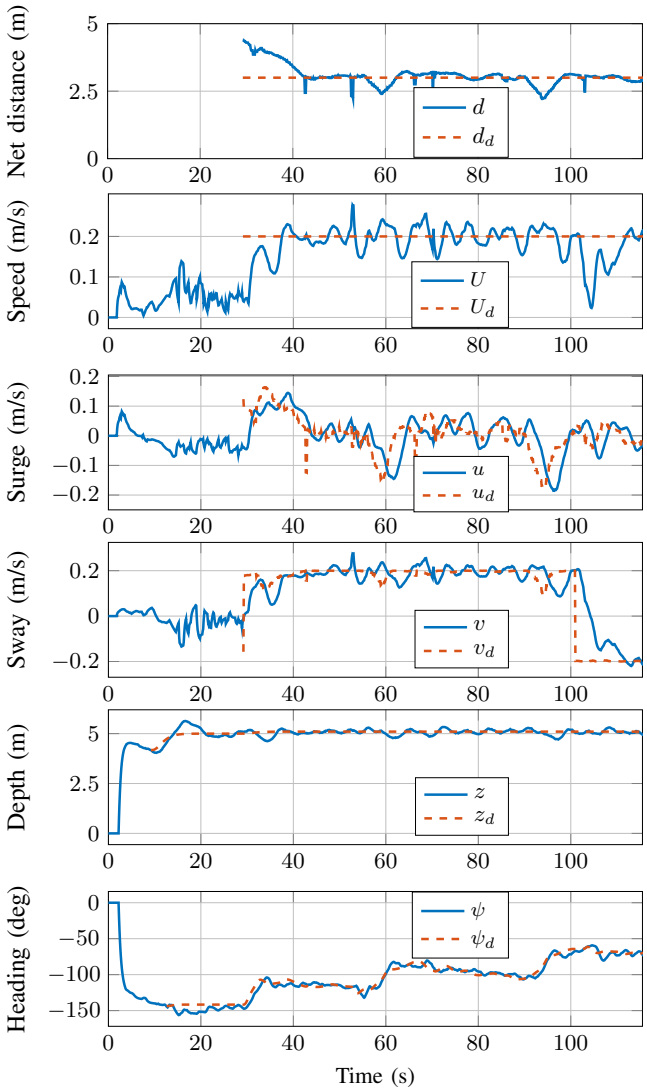

Fig. 3: Case study 1: GSTA. Measured (blue, solid line) vs. reference (red, dashed line) for distance to net, total speed, surge speed, sway speed, depth and heading.

and sway velocities, depth and heading angle with their respective reference values. For the first 29 seconds in Fig. 3, the vehicle descended to the desired depth $z_d = 5$ m. After 29 seconds, net following was activated, and the vehicle attempted to maintain the desired depth while tracking the desired heading angle and velocity references in surge and sway. After 100 seconds, the ROV was commanded to move in the opposite direction, which resulted in a change in the sway velocity reference signal. Moreover, it can be seen that the desired distance to the net was maintained and that the references for surge, sway, depth, and heading were tracked with low errors throughout the trial.

TABLE II: Adaptive GSTA controller gains

Degree of freedom	β	ω	γ	ϵ	λ	α_{tol}
Surge	6	1	5	0.0001	2	0.2
Sway	6	1	5	0.0001	2	0.2
Depth	5	1	3	0.00001	0.01	0.15
Heading	1	1	1	0.001	1	0.2

TABLE III: PID Controller gains

Degree of freedom	k_p	k_d	k_i
Surge	200	0	5
Sway	200	0	5
Depth	100	0	1
Heading	15	1	0.5

B. Case study 2: Adaptive GSTA

In the testing of the performance of the adaptive GSTA controller, the parameters displayed in Tab. II were applied for the update law used to estimate the gains. The states along with their respective reference values can be seen in Fig. 4. The vehicle spent the first 17 seconds descending towards the desired depth. After 63 seconds, the commanded direction of net-following was changed, affecting the sway velocity reference signal. While some outliers in the net-following system, likely due to the interference of fish in the DVL measurements, lead to sudden changes and spikes in the references for net distance and surge and sway velocity, the references were still tracked with low errors. From Fig. 5, it can be seen that the adaptive gains for surge, sway and yaw quickly converged towards stable values while the gain for depth had yet to converge to a stationary value at the end of the trial.

C. Case study 3: PID

The final case study aims to showcase the performance that is to be expected from using PID controllers. The gains used in this case study can be found in Tab. III and the field trial results can be seen in Fig. 6. After reaching the desired depth and activating net-following, the vehicle tracked the surge, sway and heading references with some error while maintaining the depth reference with low error. A steady-state error can be seen in sway and absolute velocity. The direction for net-following was changed after 71 seconds.

D. Summary of Results

The RMSEs for the three case studies are summarized in Tab. IV. Overall, it can be seen that the PID controller was outperformed by the GSTA controllers, although admitting a much lower RMSE in depth than the other two control methods. A steady-state error for velocity tracking was also observed with PID control. The adaptive GSTA controller performed better that the GSTA in surge, sway and depth, while being slightly worse in heading reference tracking. Nevertheless, both controllers ensured that the control objective was satisfied with low errors.

VII. Discussion

While both of the proposed GSTA controllers were capable of achieving the control objective, i.e., keeping a desired constant depth and distance to the net while tracking the

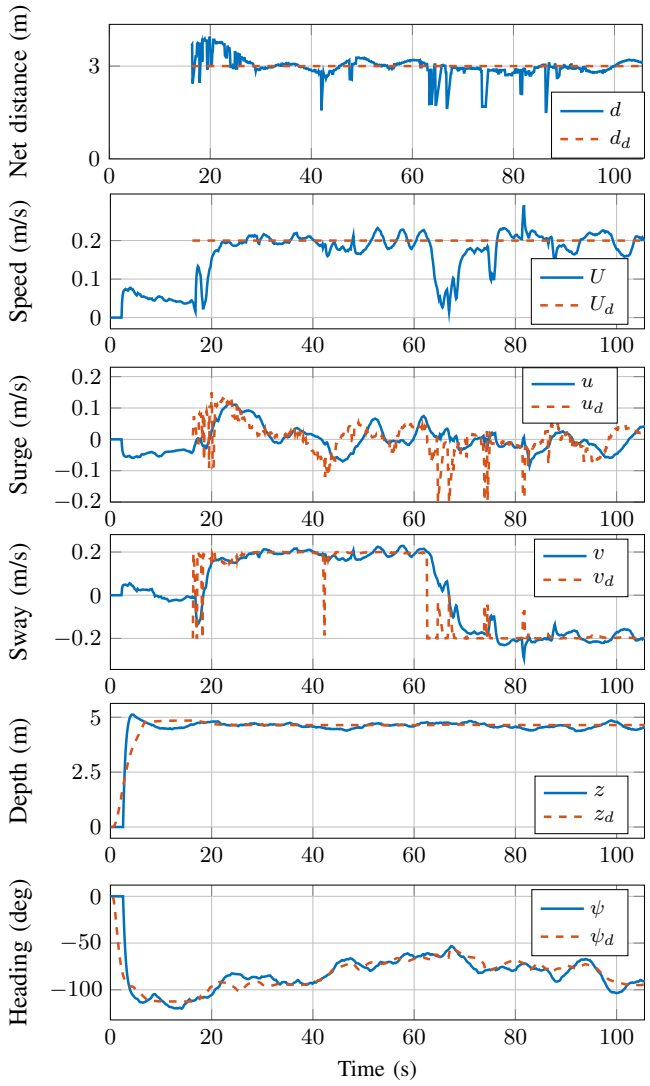

Fig. 4: Case study 2: AGSTA. Measured (blue, solid line) vs. reference (red, dashed line) for distance to net, total speed, surge speed, sway speed, depth and heading.

surge, sway and heading references, it was found that a steady-state error occurred in velocity tracking when using PID control. This negatively affected the ability of the net-following system to hold the desired distance to the net. It was also found that the adaptive GSTA slightly outperformed the fixed-gain GSTA while both of these performed better than the PID controller (except for keeping the desired depth, see Tab. IV).

While the controllers achieved the objective, they all suffered from occasional outliers in the net distance estimates. Bad net distance estimates were most likely due to fish obstructing the DVL beams, which led to sudden changes in the references, especially for the surge velocity. Moreover, the relatively low sampling frequency of the DVL (8 Hz) and the associated non-regular delays may also have a negative impact on the control performance.

Incorrect net distance estimates may thus explain some of the deviations in reference tracking performance for surge,

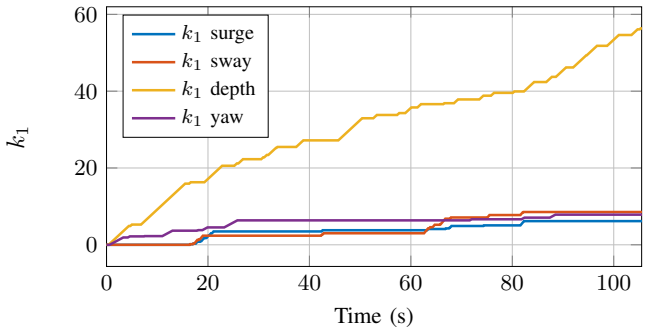

Fig. 5: The evolution of the elements of the adaptive gain matrix $\boldsymbol{k}_1$ over time for adaptive GSTA.

TABLE IV: RMSE for GSTA, adaptive GSTA and PID control.

	GSTA	Adaptive GSTA	PID
Distance to net [m]	0.402	0.681	0.820
Total speed [m/s]	0.078	0.055	0.114
Surge [m/s]	0.054	0.035	0.048
Sway [m/s]	0.077	0.046	0.103
Depth [m]	0.143	0.113	0.078
Heading [rad]	0.090	0.097	0.145

sway and heading and, in particular, the RMSE for net distance.

As with all controllers, the performance of the control laws is closely related to the tuning of the gains. The controller gains were found by in-field tuning. The adaptive GSTA can adaptively tune its gains, which is likely the reason for the superior tracking in velocity. However, it was also experienced that it was challenging to tune the terms that are responsive for calculation of the adaptive gains. Particularly, a small value for α_{tol} can lead to high-gain instability, as the gain will increase when the sliding variable leaves the sliding manifold. A very small value of α_{tol} for the depth DOF is thus the most likely cause for the rise in $k_{1,z}$, which corresponds well with the small oscillations in depth observed near the end of the trial. The superior performance of PID in depth is likely due to better tuning. It was, however, challenging to tune the PID controller for velocity control, as large values for the integral gain led to instability due to the integration of sensor noise. This resulted in conservative tuning in velocity for PID control. In any case, given more time for tuning, it is likely that the performance of all controllers would improve.

VIII. Conclusions

In this paper, we have proposed the use of two higher-order sliding mode (HOSM) control algorithms for 4DOF control of an underwater vehicle, one fixed gain and one adaptive gain GSTA. The stability properties of the controllers were analyzed and it was proved that the tracking error will converge to the origin globally and in finite-time. Furthermore, the controllers were validated in a set of field trials in an autonomous system where an underwater vehicle performed autonomous net inspection inside an aquaculture fish cage. The results have been used to compare the control laws to each other and PID control. It was found

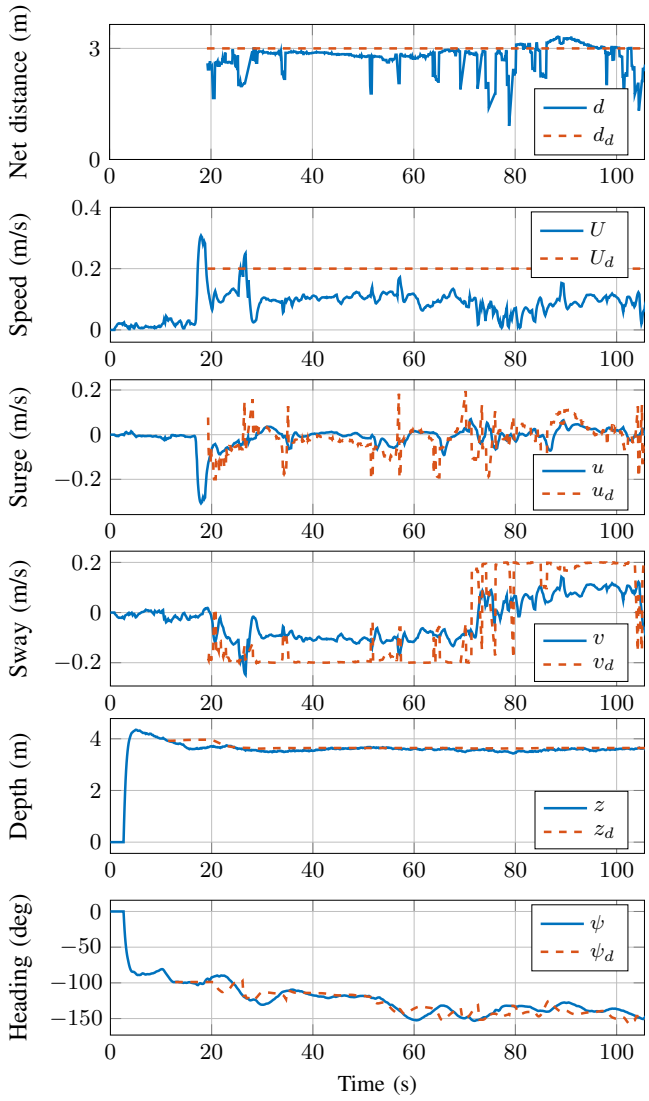

Fig. 6: Case study 3: PID. Measured (blue, solid line) vs. reference (red, dashed line) for distance to net, total speed, surge speed, sway speed, depth and heading.

the HOSM controllers demonstrated good performance in reference tracking.

ACKNOWLEDGMENT

The research was conducted at SINTEF Ocean's full-scale aquaculture facility ACE with support from the ACE team. The authors received internal funding and support from SINTEF Ocean through the RACE program. The work is partly supported by the Research Council of Norway through the project CHANGE (grant no. 313737), SFI Exposed (grant no. 237790), the Centre of Excellence funding scheme under Project 223254 - NTNU AMOS, and the European Research Council (ERC) under the European Union's Horizon 2020 research and innovation programme, through the ERC Advanced Grant 101017697-CREME.

REFERENCES

[1] Y. R. Petillot, G. Antonelli, G. Casalino, and F. Ferreira, "Underwater robots: From remotely operated vehicles to intervention-autonomous underwater vehicles," *IEEE Robotics & Automation Magazine*, vol. 26, no. 2, 2019.

[2] M. Føre, K. Frank, T. Norton, E. Svendsen, J. A. Alfredsen, T. Dempster, H. Eguiraun, W. Watson, A. Stahl, L. M. Sunde, C. Schellewald, K. R. Skøien, M. O. Alver, and D. Berckmans, "Precision fish farming: A new framework to improve production in aquaculture," *Biosystems Engineering*, vol. 173, 2018.

[3] L. C. Gansel, S. Rackebrandt, F. Oppedal, and T. A. McClimans, "Flow fields inside stocked fish cages and the near environment," *Journal of Offshore Mechanics and Arctic Engineering*, vol. 136, Aug. 2014.

[4] P. Klebert, Ø. Patursson, P. C. Endresen, P. Rundtop, J. Birkevold, and H. W. Rasmussen, "Three-dimensional deformation of a large circular flexible sea cage in high currents: Field experiment and modeling," *Ocean Engineering*, vol. 104, 2015.

[5] J.-J. E. Slotine and W. Li, *Applied nonlinear control*. Englewood Cliffs, N.J: Prentice Hall, 1991.

[6] Y. B. Shtessel, J. A. Moreno, F. Plestan, L. M. Fridman, and A. S. Poznyak, "Super-twisting adaptive sliding mode control: A lyapunov design," in *49th IEEE Conference on Decision and Control (CDC)*, 2010, pp. 5109–5113.

[7] A. Levant, "Higher-order sliding modes, differentiation and output-feedback control," *International Journal of Control*, vol. 76, 2003.

[8] ——, "Sliding order and sliding accuracy in sliding mode control," *International Journal of Control*, vol. 58, 1993.

[9] Y. Shtessel, M. Taleb, and F. Plestan, "A novel adaptive-gain supertwisting sliding mode controller: Methodology and application," *Automatica*, vol. 48, 2012.

[10] J. A. Moreno, "A linear framework for the robust stability analysis of a generalized super-twisting algorithm," in *2009 6th International Conference on Electrical Engineering, Computing Science and Automatic Control (CCE)*, 2009.

[11] I. Castillo, L. Fridman, and J. A. Moreno, "Super-twisting algorithm in presence of time and state dependent perturbations," *International Journal of Control*, vol. 91, 2018.

[12] T. I. Fossen, *Handbook of Marine Craft Hydrodynamics and Motion Control*. John Wiley & Sons, Apr. 2021.

[13] I.-L. G. Borlaug, K. Y. Pettersen, and J. T. Gravdahl, "The generalized super-twisting algorithm with adaptive gains," *International Journal of Robust and Nonlinear Control*, vol. 32, 2022.

[14] J. Guerrero, J. Torres, V. Creuze, and A. Chemori, "Trajectory tracking for autonomous underwater vehicle: An adaptive approach," *Ocean Engineering*, vol. 172, pp. 511–522, 2019.

[15] I.-L. G. Borlaug, K. Y. Pettersen, and J. T. Gravdahl, "Tracking control of an articulated intervention autonomous underwater vehicle in 6DOF using generalized super-twisting: Theory and experiments," *IEEE Transactions on Control Systems Technology*, vol. 29, 2021.

[16] B. A. Kristiansen, M. E. Grøtte, and J. T. Gravdahl, "Quaternion-based generalized super-twisting algorithm for spacecraft attitude control," *IFAC-PapersOnLine*, vol. 53, 2020, 21st IFAC World Congress.

[17] B. Sumantri, N. Uchiyama, and S. Sano, "Generalized super-twisting sliding mode control with a nonlinear sliding surface for robust and energy-efficient controller of a quad-rotor helicopter," *Proceedings of the Institution of Mechanical Engineers, Part C: Journal of Mechanical Engineering Science*, vol. 231, 2017.

[18] H. S. Fadum, "The Generalized Super-Twisting Algorithm Used for Robust Control of Unmanned Subsea Vehicles Operating at Exposed Aquaculture Sites," Master's thesis, NTNU, 2022.

[19] H. B. Amundsen, W. Caharija, and K. Y. Pettersen, "Autonomous ROV inspections of aquaculture net pens using DVL," *IEEE Journal of Oceanic Engineering*, vol. 47, 2021.

[20] P. Rundtop and K. Frank, "Experimental evaluation of hydroacoustic instruments for ROV navigation along aquaculture net pens," *Aquacultural Engineering*, vol. 74, pp. 143–156, 2016.

[21] M. Candeloro, A. J. Sørensen, S. Longhi, and F. Dukan, "Observers for dynamic positioning of ROVs with experimental results," *IFAC Proceedings Volumes*, vol. 45, no. 27, pp. 85 – 90, 2012, 9th IFAC Conference on Manoeuvring and Control of Marine Craft.